J. Phys. D: Appl. Phys. **37** (2004) L9–L12 PII: S0022-3727(04)71373-X

RAPID COMMUNICATION

Microbeam high-resolution diffraction and x-ray standing wave methods applied to semiconductor structures

A Kazimirov[1], D H Bilderback[1], R Huang[1], A Sirenko[2] and A Ougazzaden[3]

[1] Cornell High Energy Synchrotron Source (CHESS), Cornell University, Ithaca, NY 14853, USA
[2] New Jersey Institute of Technology, University Heights, Newark, NJ 07102-1982, USA
[3] Laboratoire MOPS, Supelec, 2, rue E. Belin, 57070 Metz, France

E-mail: ayk7@cornell.edu

Received 3 November 2003
Published 28 January 2004
Online at stacks.iop.org/JPhysD/37/L9 (DOI: 10.1088/0022-3727/37/4/L01)

Abstract
A new approach to conditioning x-ray microbeams for high angular resolution x-ray diffraction and scattering techniques is introduced. We combined focusing optics (one-bounce imaging capillary) and post-focusing collimating optics (miniature Si(004) channel-cut crystal) to generate an x-ray microbeam with a size of 10 μm and ultimate angular resolution of 14 μrad. The microbeam was used to analyse the strain in sub-micron thick InGaAsP epitaxial layers grown on an InP(100) substrate by the selective area growth technique in narrow openings between the oxide stripes. For the structures for which the diffraction peaks from the substrate and the film overlap, the x-ray standing wave technique was applied for precise measurements of the strain with a $\Delta d/d$ resolution of better than 10^{-4}.

High angular resolution x-ray diffraction (HRXRD) and scattering techniques have been among the major characterization tools for the semiconductor industry for more than two decades, providing important information about strain, composition, mosaic structure and defect density in thin epitaxial layers [1] and, in the case of the x-ray standing wave (XSW) method, about interface atomic structure and the location of doping and absorbate atoms relative to the host lattice [2]. In general, these techniques require an incident x-ray beam with an angular divergence less than the width of the Darwin reflection curve, i.e. <50 μrad for perfect crystals. Recent advances in technology towards further miniaturization of active electronic elements make possible production of semiconductor structure with dimensions from several microns (e.g. lasers and modulators in modern optoelectronics) to several nanometres (quantum wires and dots). Effective control of the main characteristics of these structures requires adequate characterization tools, i.e. x-ray techniques combining both high spatial and high angular resolution. Sub-micron size beams have become available recently at synchrotron radiation (SR) facilities due to the remarkable progress in x-ray focusing by using a variety of different focusing optics [3]. However, any focusing optics necessarily creates convergent x-ray beams with convergence angles of a few milliradians, deterring the development of microbeam high angular resolution techniques.

There are several approaches to overcome this problem. The first one is based on using a pinhole of a few microns size and on taking advantage of the excellent angular collimation of the beam provided by 3rd generation SR sources [4, 5]. The pinhole, however, significantly deteriorates the angular resolution due to diffraction effects, and the intensity of the microbeam is limited by the flux density of the incident beam. A highly collimated monochromatic x-ray microbeam of 7 μm by 5 μm with both vertical and horizontal divergence of 5 to 7 μrad was produced by collimating an undulator beam by slits and compressing it further with multi-crystal optics [6].

This beam was used to study lattice strain in semiconductor structures [7–9]. However, the low intensity of this beam as a result of the high monochromatization and two-dimensional collimation makes it problematic for use in intensity limited experiments such as XSW or reciprocal space mapping. To perform high angular resolution measurements, however, only collimation in the diffraction plane is required. The microbeam XSW technique has been recently demonstrated [10] based on one-dimensional vertical focusing of the undulator beam with linear parabolic lenses. An x-ray beam of 1.5 by 100 μm was used to perform XSW measurements on cleaved semiconductor heterostructures. The XSW field was generated using Bragg diffraction in the horizontal plane where high angular collimation of the undulator beam has been preserved. In this paper, we propose a new approach based on two-dimensional focusing and post-focusing collimating optics while making an effort to introduce a non-dispersive set-up, which has been for a long time the main optical scheme for high angular resolution measurements, into microbeam diffraction experiments.

The experimental set-up is shown in figure 1. Experiments were performed at the CHESS D1 bending magnet beamline. The energy of the x-ray beam was tuned to 12.5 keV (i.e. above the As-K and Ga-K absorption edges) by using a double crystal multi-layer monochromator with a band pass of 1.1%. A one-bounce imaging capillary [11] with a working distance of 30 mm and gain of 75 produced an x-ray beam with a circular size of 10 μm FWHM and a divergence of 4 mrad. A miniature Si(400) two-bounce channel-cut crystal with a channel width of 0.5 mm was designed for this experiment and inserted between the tip of the capillary and the focal spot.

The x-ray beam in front of the channel-cut crystal has a wide energy spread from the upstream multi-layer optics

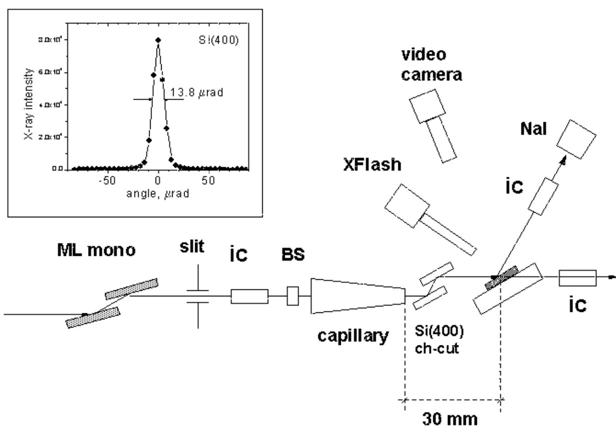

Figure 1. Experimental set-up for the microbeam high-resolution diffraction and XSW measurements at CHESS based on a one-bounce imaging capillary with a working distance of 30 mm and a beam size at the focal spot of 10 μm and a miniature Si(400) channel-cut crystal. The intensity of the incident and diffracted x-ray beams are monitored by ion chambers, IC. The beam stop, BS, is blocking the through beam. The energy dispersive XFlash detector is used to monitor fluorescence yield. The intensity of the beam diffracted from the sample is measured by the scintillation NaI detector. The sample was mounted on a computer controlled XY piezo stage with a spatial resolution of 2 nm assembled on a one-circle goniometer with the horizontal rotation axis. The inset shows the Si(400) instrumentation rocking curve.

and a wide angular spread created by the focusing capillary. To characterize the ultimate angular resolution of the optics, the (004) rocking curve from the standard Si(001) wafer was measured by rocking the Si(004) channel-cut crystal in the 4 mrad convergent beam from the capillary. A rocking curve width of 14 μrad was observed, in good agreement with the theory (inset in figure 1), demonstrating the excellent angular resolution of the set-up.

The Liouville theorem (preservation of phase space) imposes limitations on the minimum beam size for diffraction-limited focusing optics: the more narrow the acceptance angle of the collimating crystal, the larger the minimum size. Using the Airy formula as a guide [12], we can estimate that the minimum beam size in the diffraction plane for 12.5 keV x-rays varies from about 1 μm for Ge(111) to 6 μm for Si(400) collimating crystals. The beam size perpendicular to the diffraction plane should not be affected. We measured the size of the beam in both vertical (diffraction) and horizontal planes with and without the collimating crystal by scanning the edge of the epitaxial film and measuring the As-K$_\alpha$ and Ga-K$_\alpha$ fluorescence yield from the film. We observed a beam size of 10 $\pm$ 1 μm (FWHM) in both directions. Thus, within our experimental error-bars, we did not see any significant broadening of the beam by the collimating crystal in the diffraction plane.

The microbeam was subsequently used for HRXRD and XSW characterization of quaternary $In_{1-x}Ga_xAs_yP_{1-y}$ semiconductor layers grown selectively by metal organic vapour phase epitaxy (MOVPE) on stripe regions of an InP(001) substrate surrounded by a pair of SiO_2 dielectric mask stripes. Selective area growth (SAG) became recently one of the most important technological platforms for production of monolithically integrated III–V semiconductor structures such as electro-absorption modulated lasers, waveguides, amplifiers, mixers and other optoelectronic telecommunication devices. By varying the geometry of the oxide pattern, epitaxial layers with different physical properties can be grown simultaneously on the same InP wafer [13, 14]. A high spatial resolution study of both thickness and composition variations in the grown layers is crucial for understanding and modelling of the SAG process and for optimization of new optoelectronic devices. SAG structures have been studied using transmission and scanning electron microscopy and interferometry [15], by microphotoluminescence [16], and by SR-based microbeam HRXRD using compressive collimation optics [7] and a pinhole [5] and using low resolution x-ray diffraction with a phase zone plate [5]. In [17], we combined microbeam x-ray fluorescence analysis based on a multi-bounce condensing capillary with a beam size of 1 μm and the microphotoluminescence technique to measure both thickness and composition variations in ternary and quaternary SAG layers.

In this paper, we studied $In_{1-x}Ga_xAs_yP_{1-y}$ layers with parameters in the open regions of the wafer (far from the oxide mask) of $x = 0.32$, $y = 0.6$ and a thickness of 0.14 μm grown using the SAG technique in the opening between two 600 μm-long SiO_2 mask stripes. The width of the oxide stripe, $\boldsymbol{A}$, varied from 10 to 140 μm and the opening between two oxide masks, $\boldsymbol{B}$, varied from 15 to 80 μm (bottom inset in figure 2). The slit in front of the capillary was vertically

narrowed to reduce the dispersion due to the difference in the lattice constants of the Si collimating crystal and the InP sample. This lowered the intensity of the incident beam from 3×10^6 to 0.9×10^6 ph s^{-1}. The sample was mounted on a computer controlled XY piezo stage with a spatial resolution of 2 nm assembled on a one-circle goniometer with the horizontal rotation axis. The beam was positioned between the oxide masks by monitoring the As-K$_\alpha$ and Ga-K$_\alpha$ fluorescence. All diffraction scans were performed by scanning the Si(400) collimating channel-cut crystal in the focused beam produced by the capillary. For a width of the channel of 0.5 mm and the typical angular scanning range of 2 mrad the displacement of the beam position on the sample was no larger than 2 μm.

Two series of the HRXRD curves were measured, one for the structures with constant $\boldsymbol{A} = 140\ \mu$m and $\boldsymbol{B}$ changing from 80 to 20 μm and the second for $\boldsymbol{B} = 30\ \mu$m and $\boldsymbol{A}$ varying from 140 to 45 μm. The strain data deduced from the diffraction curves are in excellent agreement with the results based on our non-diffraction analysis [17]. In both series of measurements we observed the change in sign of the strain at certain $\boldsymbol{B}(\boldsymbol{A})$ values. The HRXRD curves and the strain data for $\boldsymbol{B} = 30\ \mu$m and different widths of the oxide mask are shown in figure 2. In the regions where the strain changes sign, the diffraction peaks from the substrate and the film overlap, making accurate strain measurements problematic. We demonstrate that for these structures the microbeam XSW technique can be used for more precise measurements.

The XSW technique is based on the generation in and above the crystal of an interference field as a result of the superposition of incident and Bragg diffracted x-ray waves [18]. The periodicity of the standing wave is the same as for diffraction planes, d. As the crystal is scanned through the Bragg peak, the XSW field is moved relative to the atomic lattice by $d/2$ inwards and the modulation of the secondary radiation yield (e.g. fluorescence or photoelectrons) is measured as a function of angle. The sensitivity of the XSW technique to the lattice constant mismatch depends on the thickness of the film, t_f, and the depth of the yield of the secondary radiation, t_{yi} [19–22]. When the fluorescence is collected from the entire thickness of the film ($t_{yi} = t_f$), the standing wave loses its 'coherence' with the atomic lattice of the film at the mismatch of $\Delta d/d > d/t_f$ and the XSW response curve becomes $1 + R(\theta)$ ($R(\theta)$ is the reflectivity curve) and not sensitive to changes in $\Delta d/d$. In the range of $\Delta d/d < d/t_f$, where the x-ray diffraction curve is not sensitive to $\Delta d/d$ due to the overlap of the weak film peak with the strong substrate peak, the XSW method can be used for accurate strain measurements [21, 22].

Two adjacent structures with $\boldsymbol{B} = 30\ \mu$m and $\boldsymbol{A} = 60$ and 70 μm were chosen for further study where the diffraction curves indicated an opposite sign of strain. The fluorescent spectrum from the sample was collected for each angular point of the rocking curve while performing multiple angular scans through the Bragg (004) peak. Simultaneously, the intensity of the Bragg reflected x-ray beam was monitored with a NaI detector equipped with a 1.5 mm thick Al attenuator. The XSW scans were performed by scanning the Si(400) channel-cut crystal. The fluorescence yield and x-ray curves were normalized by the angular distribution of the incident beam intensity after the channel cut. The XSW data collected from one of the probed structures ($\boldsymbol{A} = 70\ \mu$m) is shown in figure 3. Enhancement in the As-K fluorescence yield from the film is clearly observed due to the shift of As atoms into the region of the stronger standing wave field, indicating the presence of a positive ($\Delta d/d > 0$) strain in the film.

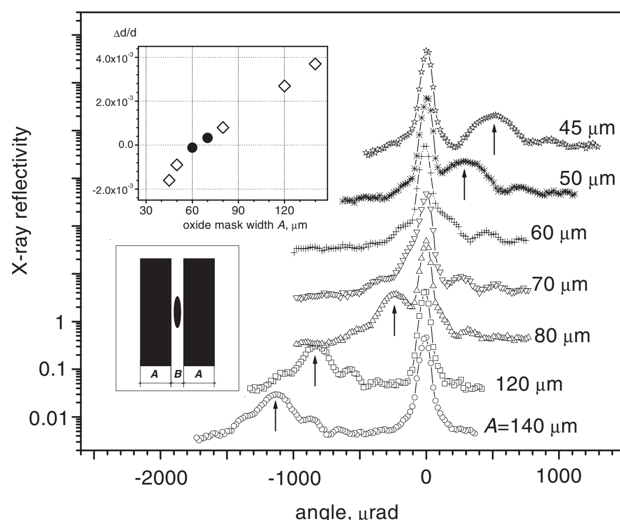

Figure 2. Experimental HRXRD curves from the quaternary $In_{1-x}Ga_xAs_yP_{1-y}$ SAG layers grown in a 30 μm wide ($\boldsymbol{B}$) area between two 600 μm-long SiO_2 mask stripes measured for different values of the SiO_2 mask width, $\boldsymbol{A}$. The positions of the SAG layer peaks are indicated. The scans were performed by scanning the channel-cut crystal in the convergent focused beam. The strain data determined from the diffraction (◇) and the XSW (●) experiments are shown in the upper inset. The bottom inset shows the top view of the structure (not to scale) with shaded rectangular SiO_2 areas and the oval beam footprint.

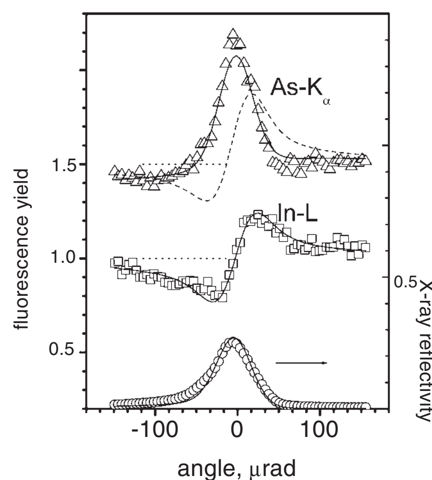

Figure 3. The experimental x-ray rocking curve and the XSW As-K and In-L fluorescence yield from the $In_{1-x}Ga_xAs_yP_{1-y}$ SAG structure grown in a 30 μm-wide area between 70 μm-wide oxide masks. The best fit (——) corresponds to fitting parameters of a layer static Debye–Waller factor of $e^{-Wst} = 0.98$ and strain $\Delta d/d = 3.28 \times 10^{-4}$ for the As-L yield curve and a substrate static Debye–Waller factor of $e^{-Wst} = 0.96$ and a yield depth of 1.7 μm (fluorescence exit angle of 24°) for the In-L yield XSW curve. The dotted horizontal lines show off-Bragg normalized yield. For comparison, the dash curve shows As-K fluorescence yield from the structure with zero strain.

The experimental As-K and In-L fluorescence yield curves were analysed by a computer program based on the dynamical theory of the x-ray diffraction and XSW in multi-layered crystal systems [23]. The In-L fluorescence originates mainly from the InP substrate. To fit the In-L fluorescence yield, we used the substrate static Debye–Waller factor, $e^{-W_{st}}$, and the depth of the In-L yield as fitting parameters. The convolution with a Gaussian function of the fluorescence yield and the reflectivity curves was used to account for dispersion. The fit yielded a very reasonable value of $e^{-W_{st}} = 0.96$ ($e^{-W_{st}} = 1.0$ for ideal lattice). The excellent fit to the experimental data indicated well-controlled standing wave behaviour and validated the proposed experimental scheme. Next, the As-K fluorescence yield from the SAG layers was fitted by using two fitting parameters, the strain ($\Delta d/d$) and the film static Debye–Waller factor. We assumed fixed layer thickness values of 0.231 μm for $\boldsymbol{A} = 70\,\mu$m and 0.217 μm for $\boldsymbol{A} = 60\,\mu$m determined in [17]. The strain data determined by the XSW measurements, $\Delta d/d = 3.3 \times 10^{-4}$ for $\boldsymbol{A} = 70\,\mu$m and $\Delta d/d = -1.1 \times 10^{-4}$ for $\boldsymbol{A} = 60\,\mu$m, are shown by filled circles in the inset in figure 2. Finally, a weak contribution to the In-L yield from the small amount of In atoms in the layer was taken into account by adjusting the depth of the In-L yield. The final fit for the structure with $\boldsymbol{A} = 70\,\mu$m is shown in figure 3. The dash curve shows As-K fluorescence yield from the layer with zero strain, demonstrating the sensitivity of the XSW method.

In conclusion, we have demonstrated that an x-ray microbeam well suited for high-resolution x-ray diffraction and XSW techniques can be produced by combining focusing optics with post-focusing collimation optics. Post-focusing collimating crystals can be designed individually for the needs of a particular experiment and the type of the crystal under study to achieve maximum flux on the sample and/or minimum size of the beam when diffraction-limited optics situations are encountered. The possibility of performing scans by scanning a channel-cut crystal in the converging focusing beam significantly simplifies experiments. We used a microbeam with a 10 μm size produced by a focusing capillary and miniature Si(400) channel-cut crystal to apply the HRXRD and XSW techniques in the study of strain in quaternary $In_{1-x}Ga_xAs_yP_{1-y}$ semiconductor layers grown on a InP(001) substrate by the SAG technique. The experimental approach developed in this paper has potential application for future analysis of micron and sub-micron size microelectronic device structures. It can also be applied to other microbeam techniques that require high angular resolution such as reciprocal space mapping, reflectometry and ultra-small angle scattering using Fresnel zone plates, refractive lenses, KB mirrors and capillaries to create the microbeams.

Acknowledgments

This work is based upon research conducted at the Cornell High Energy Synchrotron Source (CHESS), which is supported by the National Science Foundation and the National Institutes of Health/National Institute of General Medical Sciences under award DMR 9713424.

References

[1] Bowen D K and Tanner B K 1998 *High Resolution X-Ray Diffractometry and Topography* (London: Taylor and Francis)
Holý V, Pietsch U and Baumbach T 1999 *High-Resolution X-Ray Scattering from Thin Films and Multilayers (Springer Tracts in Modern Physics)* p 149
[2] Zegenhagen J 1993 *Surf. Sci. Rep.* **18** 199
[3] Riekel C 2000 *Rep. Prog. Phys.* **63** 233–62
[4] Eastman D E, Stagarescu C B, Xu G, Mooney P M, Jordan-Sweet J L, Lai B and Cai Z 2002 *Phys. Rev. Lett.* **88** 156101
[5] Cai Z-H *et al* 1999 *Appl. Phys. Lett.* **75** 100
[6] Tsusaka Y, Yokoyama K, Takeda S, Urakawa M, Kagoshima Y, Matsui J, Kimura S, Kimura H, Kobayashi K and Izumi K 2000 *Japan. J. Appl. Phys.* **39** L635
[7] Kimura S *et al* 2000 *Appl. Phys. Lett.* **77** 1286
[8] Yokoyama K *et al* 2002 *Japan. J. Appl. Phys.* **41** 6094
[9] Matsui J, Tsusaka Y, Yokoyama K, Takeda S, Urakawa M, Kagoshima Y and Kimura S 2002 *J. Cryst. Growth* **237–239** 317
[10] Drakopoulas M, Zegenhagen J, Snigirev A, Snigireva I, Hauser M, Eberl K, Aristov V, Shabelnikov L and Yunkin V 2002 *Appl. Phys. Lett.* **81** 2279
[11] Bilderback D H and Fontes E 1997 *AIP Conf. Proc.* **417** 147
[12] Attwood D 1999 *Soft X-Rays and Extreme Ultraviolet Radiation: Principles and Applications* (Cambridge: Cambridge University Press)
[13] Mason B *et al* 2002 *IEEE Phot. Tech. Lett.* **14** 27
[14] Sudo S, Kudo K, Mori K and Sasaki T 2001 *Conf. Proc. International Conf. on InP and Related Materials (IPRM' 2001)* p 390
[15] Gibbon M, Stagg J P, Cureton C G, Thrush E J, Jones C J, Mallard R E, Pritchard R E, Collis N and Chew A 1993 *Semicond. Sci. Technol.* **8** 998
[16] Alam M A *et al* 1999 *Appl. Phys. Lett.* **74** 2617
[17] Sirenko A A, Reynolds C L, Peticolas L J, Ougazzaden A, Kazimirov A, Huang R, Fontes E and Bilderback D 2003 *J. Cryst. Growth* **253** 38
[18] Batterman B W 1969 *Phys. Rev. Lett.* **22** 703
[19] Andersen S K, Golovchenko J A and Mair G 1976 *Phys. Rev. Lett.* **37** 1141
[20] Kohn V G and Kovalchuk M V 1981 *Phys. Status Solidi* a **64** 359
[21] Kazimirov A Yu, Kovalchuk M V and Kohn V G 1988 *Sov. Tech. Phys. Lett.* **14** 587
[22] KazimirovA, Zegenhagen J and Cardona M 1998 *Science* **282** 930
[23] Kohn V G 2002 *Phys. Status Solidi* b **231** 132